Polymer Nanocomposites with a Low Thermal Expansion Coefficient

YuanQiao Rao* and Thomas N. Blanton

Research Laboratories, Eastman Kodak Company, 1999 Lake Avenue, Rochester, New York 14650-2158

ABSTRACT: In this paper, a PEO−clay(PVP) nanocomposite was designed and the nanocomposite film was produced. The film exhibits a low thermal expansion coefficient of ∼10 ppm/°C, which is similar to that of metals. The film also exhibits an unexpected high heat distortion temperature, which is much higher than the melting point of polyethylene oxide (PEO), as well as a much improved O_2 barrier property, high stiffness, and high strength. The significant property improvements are related to the structure of the formed composite. In this composite, the clay crystal is first intercalated by polyvinyl pyrrolidone (PVP), which regulates the stacking of the clay sheets and forms a well-ordered intercalated clay crystal. This intercalated clay crystal directs the crystallization and crystal orientation of the PEO in the composite. The property change with the amount of clay added suggests that there is a critical clay loading of ∼10 vol % beyond which the polymer based composite exhibits superior properties.

Introduction

Materials typically expand when heated. The expansion is characterized by the volumetric or linear thermal expansion coefficient. The three primary types of materials expand differently. Polymers expand more than metals, and metals expand more than ceramics. The linear thermal expansion coefficient of polymers is in the range of 20−100 ppm/°C,[1] that of metals is in the range of 3−20 ppm/°C,[2,15] and that of ceramics is in the range of 3−5 ppm/°C.[3]

The high value of the thermal expansion coefficient of polymers is caused by the low energy barrier for the chain conformation to be changed.[4] Different approaches have been applied to reduce the thermal expansion in polymeric materials, including crystallization,[5,6] improved chain orientation,[7] crosslinking,[8] and the addition of fillers of low thermal expansion.[9−11] These studies led to some semiempirical equations to predict the thermal expansion coefficient of a two-phase material: Turner's equation,[11] Halpin−Tsai's equation,[12] Fahmy−Ragai's equation,[9,10] Chow's work,[13] and more recent work by Paul's group,[14] just to name a few. These studies also showed experimentally and theoretically that, in order to reduce the thermal expansion coefficient of the polymeric material to be near that of metals or ceramics, continuous fiber or filler that has an aspect ratio of higher than 100 and a low-thermal expansion coefficient is needed.[9−14] This requirement implies that the constructed material lacks optical transparency unless a nanosized filler is used.

There have been many studies exploring the effect of the incorporation of nanoparticles, of different chemical nature, size, and shape, on the thermal properties of polymers.[16−36] Extensive studies were carried out on nanoclay−polymer nanocomposites because of the high aspect ratio and the low cost of the nanoclay; however, these nanocomposites have a limited reduction in their thermal expansion coefficient.[16−24] The lack of significant improvement is in agreement with some empirical predictions. It was attributed to the difficulty to achieve exfoliation of the nanoclay.[23] Although various commercial successes have been achieved using nanocomposites, in particular nanoclay-based nanocomposites, some fundamental understanding regarding the structure−property relation in the nanocomposite remains elusive. It is our objective to better understand the governing rules of nanocomposites through rationally designing and constructing the nanoclay-based nanocomposite and characterizing its structure and properties. For this purpose, we made a nanocomposite with a controlled high-order structure using montmorillonite nanoparticulates, polyvinyl pyrrolidone (PVP), and polyethylene oxide (PEO) and studied its thermal properties.

The material design in this paper is based on a wealth of information from previous studies. Montmorillonite nanoparticulate is an interesting clay nanoparticle.[37] A single sheet of montmorillonite comprises two layers of a two-dimensional array of silicon−oxygen tetrahedral on the outside and one layer of a two-dimensional array of an aluminum− or a magnesium−oxygen−hydroxyl octahedral in the center. The unit cell of a montmorillonite crystal has a characteristic (001) basal spacing of at least 9.2 Å. The sheets of the a−b crystal plane have a negative charge and hydroxyl groups linked to aluminum or magnesium. The cohesive force between layers is primarily electrostatic and susceptible to cleavage. It is an ideal nanoparticle for nanocomposite study. Either the clay crystal can be used as the nanoparticulate, which is often called intercalated clay, or the single sheet of clay can be used, which is called exfoliated clay. The hydroxyl groups and charges on the particles allow the control of the interaction between the nanoparticles and the polymer matrix. The individual clay sheet typically has an aspect ratio higher than 100, which is highly desired according to conventional composite theories. Pioneering work at Toyota showed that polymer−clay nanocomposites have a combined enhancement of modulus, strength, and toughness.[38−40] The clay nanocomposite was also shown to have improved flame retardance[39] and barrier properties.[16,42]

Research on the structure of the nanoclay-based composite is actively being pursued. Many researchers have studied the structure of the clay nanocomposite containing PEO and PVP.[43−46] The strong absorption of these two polymers on the clay surface was observed but the mechanism is still not well understood.[43−45] It has been shown that the PEO chains residing inside the clay interlayer do not have cooperative glass transition motions when they are confined in an 8 Å interlayer spacing.[47] In situ SAXS was used to study the structural change of a PEO−clay composite upon heating, and the irreversible melting of

* To whom correspondence should be addressed. E-mail: yuanqiao.rao@kodak.com.

10.1021/ma7020216 CCC: $40.75
Published on Web 12/29/2007

PEO crystals was observed in the composite.[48] A clay−PEO nanocomposite comprising of a Laponite clay was shown to possess oriented multilayers on the micrometer length scale.[49] The secondary crystallization of PEO was detected in an organoclay−PEO nanocomposite using synchrotron X-ray diffraction.[50] The clay has been shown to influence the crystallization and the crystal orientation of PEO.[51,52] PVP is one of the few polymers that intercalates the clay well.[43−45,53] It was shown that the d-spacing increases linearly with the amount of PVP up to exfoliation.[43−45] It is our intent to explore the possibility of modulating the high-order composite structure through surface PVP absorption and to study the structure property relation of these new PEO−clay(PVP) nanocomposites.

Experimental Section

Montmorillonite clay, NaCloisite, was supplied by Southern Clay Products and used as received. It has a reported aspect ratio (length/thickness, *L*/*t*) of 200 and a density of 2.6 g/cm^3. Polyethylene oxide, POLYOX W-750, which has a molecular weight of 300 000 and a density of 1.1 g/cm^3, was supplied by Dow Chemical (Midland, MI). Polyvinylpyrrolidone, PVP10K, with a density of 1.2 g/cm^3, was obtained from BASF. A 3 wt % aqueous NaCloisite dispersion was made using a high-shear mixer. The dispersion was further centrifuged and filtered to remove impurities and big particles. This clay dispersion remained well dispersed without settling for several months. PVP was then added to the clay dispersion at different PVP/clay ratios and stirred for 1 h. PEO was slowly added to the mixture under vigorous mixing. The mixture was put together based on a desirable weight ratio. The corresponding volume ratio was then calculated based on the densities and used in the results and discussion. The resultant dispersion was coated using a doctor blade on a substrate. The coating was first dried at 50 °C for 10 min, followed by drying in a vacuum oven at room temperature overnight. A freestanding film of ∼30 μm was peeled from the substrate. The samples were conditioned at 25 °C/50% relative humidity (RH) before further testing.

The structure of the nanocomposite film was investigated by X-ray diffraction (XRD), differential scanning calorimetry (DSC), and transmission electron microscopy (TEM). For XRD analysis, a Rigaku RU-300 Bragg−Brentano diffractometer with a scintillation point detector and a Bruker GADDS microdiffractometer with a 2D area detector were used. Crystal sizes of clay and PEO were calculated using the Scherrer equation.[55] In the calculation, the (001) peak of clay crystal was used to calculate the crystal size perpendicular to the clay sheet and the (120) and (032) peaks of the PEO crystal were used to calculate the 3D crystal dimensions. DSC analyses were performed using a Perkin-Elmer DSC 7, and a Joel 2000 TEM was used to obtain electron micrographs. The oxygen barrier properties of coatings were measured using a MOCON OX-TRAN 2/21 according to ASTM F392. The longitudinal thermal expansion coefficient and thermal distortion temperature were measured by thermal mechanical analysis using TMA 2940 (TA Instruments). The thermal expansion coefficient was measured when the sample was cooled at a rate of 5 °C/min after being heated first to 150 °C and equilibrated for 5 min for composites and to 60 °C for pure polymers. The heat distortion temperature was defined by the temperature at which the sample dimensional change was higher than 1% under a stress of 400 kPa. The mechanical properties were measured using a Sintech tester according to ASTM D882-80a. At least three samples were tested, and the coefficient of variance was within 10% for all measurements. All ambient temperature measurements were conducted at 50% RH.

Results and Discussion

Absorption and Ordering in PVP−Clay Composites. PVP−clay composite films of different PVP/clay ratios were made. XRD spectra show that the d-spacing of clay increases with the amount of added PVP as listed in Table 1, which is consistent with previous studies.[43−45]

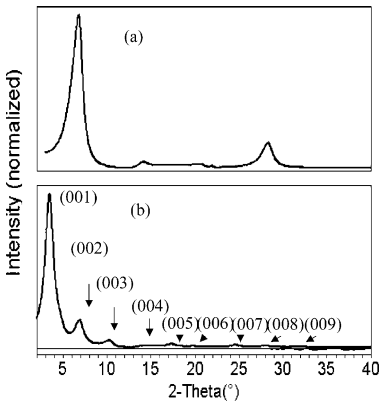

Figure 1. X-ray diffraction patterns, reflection mode geometry, for (a) Cloisite Na$^+$, (b) PVP−Cloisite Na$^+$ nanocomposite, 48/52 vol %.

Table 1. XRD Results of Clay Basal Spacing at Different PVP Loadings

PVP (vol%)	d-spacing (Å)
0	13
35	18.1
48	25.5
68	32.7

Table 2. Crystallite Size and Paracrystalline Parameter for Cloisite Clay Crystal

	L (Å)	g_{II}
neat Cloisite Na$^+$	57	0.68
Cloisite Na$^+$ in 48/52 PVP−clay composite	105	0.16

Figure 1 shows that a total of nine orders of (00*l*) Bragg diffraction peaks of clay crystals appears in one PVP−clay composite film of 48 vol % PVP. Usually in an intercalated state, the clay (001) basal plane diffraction peak broadens as a result of increased disorder in the clay crystal.[53] The appearance of the higher-order clay diffraction peaks in the PVP−clay indicates a much more perfect stacking in clay crystals. The degree of perfection of the intercalation spacing can be analyzed using the concept of the crystallite size and paracrystalline parameter according to the following equation:[54]

$$(\delta_s)_0^2 = (\delta s)_c^2 + (\delta s)_{II}^2 = \frac{1}{L_{hkl}^2} + \frac{(\pi g_{II})^4 n^4}{d_{hkl}^2} \qquad (1)$$

in which δ_s is the broadening of the diffraction peak, L is the crystal size, g_{II} is the paracrystalline parameter, n is the order of the diffraction peak, and d_{hkl} is the d-spacing of the (*hkl*) diffraction peak. The larger L is, and the smaller g_{II} is, the more perfect the crystal. Table 2 lists the crystallite size and paracrystalline parameter of the neat Cloisite Na$^+$ clay and the PVP-intercalated clay crystal. The basal spacing of neat Cloisite Na$^+$ clay is 13.1 Å and is higher than the reported data of 9.6 Å for dried clay due to absorbed water. It is seen that the g_{II} of the PVP-intercalated clay crystal is much smaller than that of the neat clay crystal. When the basal spacing of 13.1 Å for the neat Cloisite Na$^+$ clay and 25.4 Å for the polymer−clay are considered, the crystallite size listed in Table 2 suggests that there are, on average, five layers of silicate sheets in one crystal in both the pure clay and the polymer−clay crystal.

It is important to understand how the polymer is absorbed on the clay and formed the above structure. It is our speculation that water plays an important role. Although the swelling of

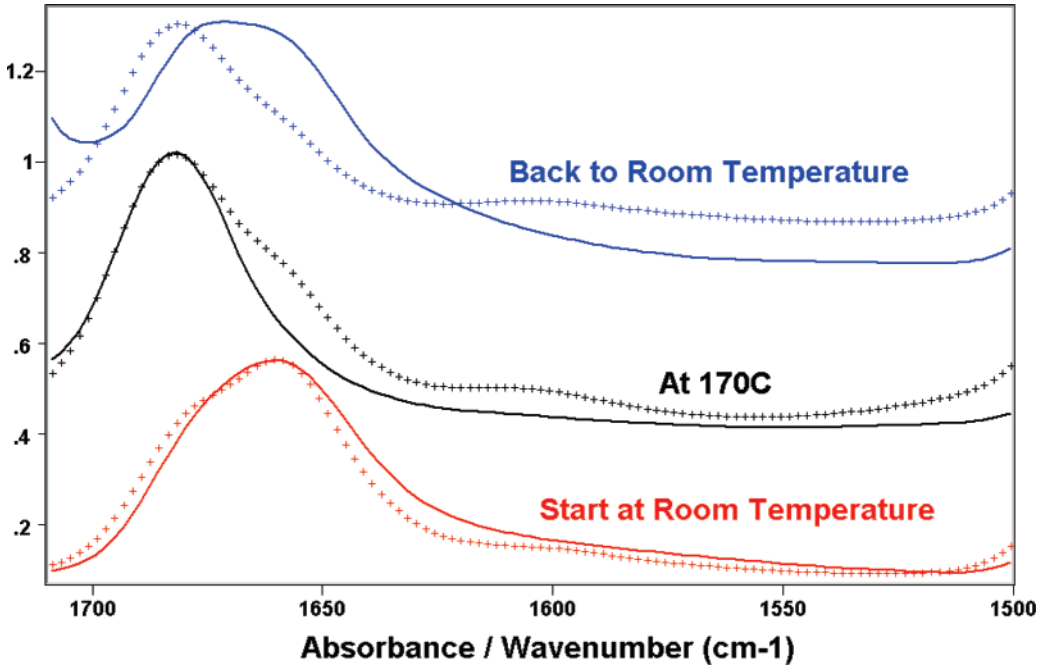

Figure 2. Infrared data at different temperatures by ATR; the — line is the polymer film, and the + + + line is the composite film.

the montmorrilonite clay was studied as early as 1933, the mechanism is still not well understood.[55] A recent work by Karaborni[56] showed that the water can either enter the hexagonal cavity and form hydrogen bonding with the OH groups inside the clay molecule or forms hydrogen bonding with the surface oxygen. To further investigate the interaction between the polymer and clay, FTIR spectra of the polymer and composite films were examined in situ upon heating the samples to a temperature of 60, 100, and 170 °C and cooling down to room temperature. The result is shown in Figure 2. Figure 2 compares the spectra of C═O vibration in PVP of both the polymer film and composite film at different temperatures. The C═O vibration has a characteristic peak around 1660−1680 cm^{-1}. At room temperature, the major peak appears about 1660 cm^{-1} for both films. The room-temperature peak is broad because of the presence of the hydrogen bonding between the water and polymer.[57] The peak maximum wavenumber and shape change for both films upon heating. The peak wavenumber of the polymer film moves to a higher wavenumber of 1682 cm^{-1}, and the peak also narrows. The change is caused by the removal of water. However, when the composite film is heated, the peak remained much broader than that of the polymer film although the major peak shifts to a higher wavenumber of 1682 cm^{-1}. The peak at 170 °C of the composite film suggests that the lower wavenumber peak, which centers around 1660 cm^{-1} remains upon heating. When two films are cooled down, the C═O vibration peak of the polymer film recovers upon absorbing water again, while that of the composite film remains similar to that at 170 °C. The retention of the low-wavelength peak suggests that there is still hydrogen bonding in the composite film even at 170 °C. It is possible that the polymer forms hydrogen bonding with the OH groups at the edges or when the polymer is strongly absorbed to the clay surface, the pendant group diffuses into the surface and has access to the OH− groups in the octahedral layer in the clay crystal. It is seen that this type of interaction is strong and stable toward heating. This would be important for stress transfer when the composite film is loaded.

Assuming PVP is absorbed to the surface of the clay in a layered fashion, the d-spacing of the intercalated clay is plotted against the number of layers of absorption in Figure 3. It shows that the thickness of a single layer of absorbed PVP is 6.5 Å. The absorption force of the PVP is comparable to that of water such that the number of layers in a clay crystal does not change after PVP intercalation. Rather, the clay crystal becomes a better-ordered structure because of the PVP absorption. However, the actual absorption mechanism still needs to be investigated, especially when the number of polymer layers between two clay sheets is over two.

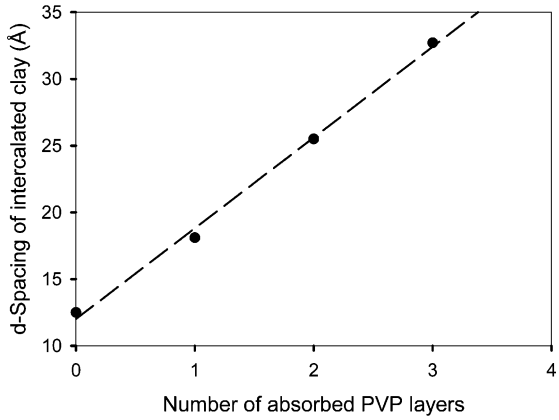

Figure 3. The change of d-spacing in an intercalated clay with the number of layers of the absorbed intercalants; ● represents the experimental data and the − − − line is the regressed line.

It is our belief that this newly formed clay crystal can be a new form of nanofiller to be used in nanocomposites because it comprises a polymer of good mechanical and thermal properties and it has a well-ordered structure. In this paper, this PVP-intercalated clay crystal was mixed with PEO for further structural control and property enhancement.

Properties of PEO−Clay(PVP) Nanocomposites. The intercalated clay with 48 vol % PVP was chosen as the new nanofiller. It was blended with different amounts of PEO to form PEO−clay(PVP) nanocomposite films. Their mechanical, thermal, and barrier properties were studied.

Table 3 shows that the PEO−clay(PVP) nanocomposite films are much stiffer and stronger than that of pure PEO films. The

Table 3. Mechanical Properties of Peo−Clay(PVP) Nanocomposite Films

clay content (vol %)	break elongation (%)	Young's modulus (GPa)	break strength (MPa)
0.0	59.5	0.8	10.6
0.4	50	0.7	10.6
1.3	19.9	1.2	9.9
2.2	12.9	2.2	14.7
4.5	9.8	3.6	15.7
12.5	1.1	6.2	23.3

Table 4. O_2 Permeability of Peo−Clay(PVP) Nanocomposite

clay content (vol %)	permeability (cm^3 cm/m^2/day)
0	>8.128
12.2	0.03

Table 5. Linear Thermal Expansion Coefficient and Heat Distortion Temperature of PEO−Clay(PVP) Nanocomposite Films

clay concn (vt %)	PVP (vt %)	thermal expansion coefficient (ppm/°C)	heat distortion temp (°C)
0	0	117	65
0	12	51.7	65
6	6	51.5	150
10	9	15.7	>200
12	12	12.2	>200
19	18	10.9	>200

modulus increases by eight times with 12.5 vol % of clay, and the strength doubles. However, the elongation to break decreases and the material becomes less tough.

Table 4 shows that PEO−clay(PVP) nanocomposite films have a much-improved O_2 barrier property. There is a 400 times reduction in O_2 permeability with 12.5 vol % clay. It is speculated that the great improvement originates from the structure of the nanocomposite, which will be discussed in detail later.

Table 5 lists the linear thermal expansion coefficient and the heat distortion temperature of PEO−clay(PVP) nanocomposite films. It is seen that the thermal expansion coefficient of the nanocomposite film is lowered to ~10 ppm/°C at a clay loading of 10 vol %. In addition, the heat distortion temperature increases to 200 °C from 65 °C, which is the melting point of the PEO. Although the PEO crystal was seen to melt via DSC measurement upon heating above 70 °C, the film still maintains its integrity under load up to 200 °C, which is 130 °C higher than the melting point of the major phase of the composite. The film is also transparent and has a transmission of 80%. One deficiency of the PEO−clay(PVP) film is the potential sensitivity to water or moisture. Both PEO and PVP are water-soluble and clay is water swellable. The composite film was immersed in water. The film property does not change after being taken out in one week and dried. The film eventually lost its integrity after several months in water. These results suggest that the moisture sensitivity of the composite film is greatly reduced, but the material is still prone to the attack of water molecules. In order to develop better materials for use, further effort is needed to explore other hydrophobic materials. It is our speculation that in the formation of the composite in this paper, water first hydrates the surface of the clay and opens up the gallery. Afterward, the PVP chain is drawn into the gallery and a strong polar interaction and possibly hydrogen bonding forms with the clay. Therefore, if a polar polymer and a solvent that can swell the clay are used, this process might be used for other matrix polymers.

Conventionally, it has been shown that continuous fibers or fillers of low-thermal expansion that have an aspect ratio of higher than 100 are needed in order to reduce the thermal

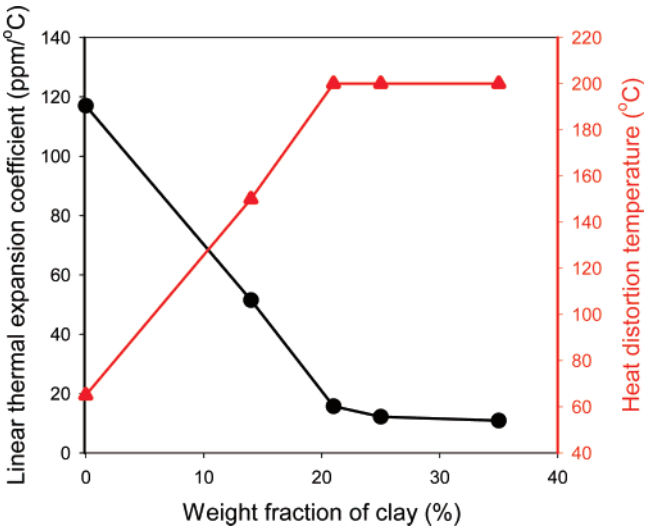

Figure 4. Thermal properties of PEO−clay(PVP) nanocomposite films: the black circle represents the linear thermal expansion coefficient, and the red triangle represents the heat distortion temperature.

expansion coefficient of the polymeric material to be near that of metals or ceramics. [9−14] There have been many studies on lowering the thermal expansion coefficient of polymers using clay.[16,20,23,24] However, the produced nanocomposites typically have a linear thermal expansion coefficient in the range of 30−40 ppm/°C. The limited reduction in the thermal expansion coefficient of the nanocomposites was attributed to the difficulty of generating the fully exfoliated clay sheet such that the apparent aspect ratio of the filler is lower than desired.[23]

Clay exfoliation has widely been the objective of many clay−polymer nanocomposite studies. It is believed that the exfoliation renders the ultimate property enhancement while partial intercalation hampers the level of improvement. Exfoliation indeed was shown to drive the property of the nanocomposites.[58] However, it is our understanding that while the state of clay (primary particle) is important to the composite, the higher order structure can be more crucial. In the case of PEO−clay(PVP) nanocomposites, it is clear that exfoliation does not occur. To the contrary, more ordered intercalation is present in the nanocomposite. The apparent aspect ratio of the intercalated clay is ~20 based on the calculated clay crystal size, much less than the expected 200. Therefore, significant improvements in properties that were observed cannot be explained by only the effect of continuum mechanics. Figure 4 plots the change in the thermal expansion coefficient and heat distortion temperature with the amount of added clay. These data suggest that there is a critical clay loading when the property of the composite experiences an abrupt change. The structural investigation and the effort of correlating the property with the structure will be discussed.

Structure of PEO−Clay(PVP) Nanocomposites and Its Relation with Properties. PEO−clay(PVP) nanocomposites discussed in the paper demonstrate good properties of a low thermal expansion coefficient, high heat distortion temperature, high modulus and strength, and low O_2 permeation. It is important to understand the structure of the nanocomposite and origins of the property improvement.

When PEO was blended with PVP−intercalated clay, the final film had an identical XRD spectrum as that of the PVP−intercalated clay in the reflection mode (Figure 1). This result suggests that the PVP−intercalated clay crystal remained intact during blending. One interesting feature of the PEO based composite diffraction pattern is the absence of any PEO

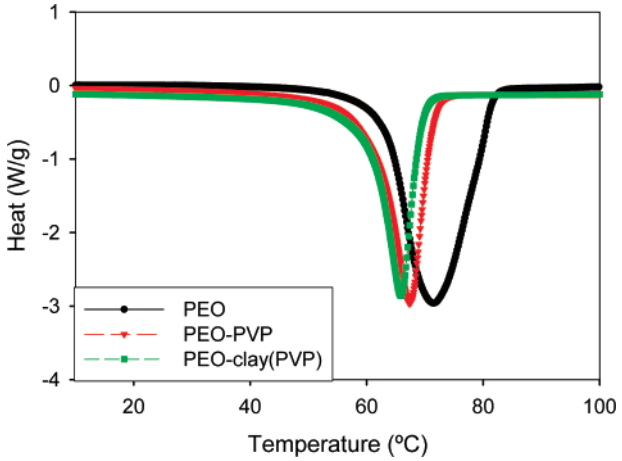

Figure 5. DSC scans of films of PEO (black circle), PEO−PVP of 87/13 volume ratio, (red triangle) and PEO−clay(PVP) of 76/12(11) volume ratio (green square).

diffraction peaks, which suggests that PEO does not crystallize in this composite. However, a DSC scan of the PEO−clay-(PVP) film as shown in Figure 5 (green square) indicates that the PEO in the clay nanocomposite is highly crystalline. On the basis of a heat enthalpy of 180 J/g for a PEO crystal,[1] 70% of the PEO in the nanocomposite (65 wt % PEO) is crystalline, which is comparable to the crystallinity of PEO in a PEO−PVP polymer film made with no clay under the same condition (Figure 5, red triangle). Figure 5 further shows that the melting point of PEO crystals in both PEO−PVP and PEO−clay (PVP) films moves to a slightly lower temperature.

Two-dimensional (2D) XRD patterns were collected to determine if additional orientation effects existed in the nanocomposite film that would explain the contradiction in the reflection mode XRD and DSC data. In Figure 6a, the 2D XRD pattern for a Cloisite Na^+ film, with the film edge perpendicular to the X-ray beam, is shown. Diffraction arcs, characteristic of a preferred orientation, are in the equatorial direction and are equivalent to the (00*l*) diffraction peaks detected by the point detector in Figure 1a. There is also a weak meridional arc seen in Figure 4a, the result of a (*hk*0) clay lattice plane. In Figure 6b, the 2D XRD pattern for the nanocomposite with the film edge perpendicular to the X-ray beam shows several equatorial arcs representing several (00*l*) diffraction peaks as seen in Figure 1b. However, there are additional high-intensity meridional-positioned diffraction arcs seen in Figure 6b, which were not observed in the reflection mode diffraction pattern (Figure 1b) collected using a point detector. If we change the alignment of the film and position it with the film surface perpendicular to the X-ray beam, a 2D XRD pattern is obtained (Figure 6c) and is dominated by two high-intensity diffraction rings. Diffraction rings are observed in XRD patterns when the orientation of the representative lattice planes is random. The two high-intensity rings in Figure 6c are due to diffraction from the PEO (120) and (032) diffraction planes. Going back to Figure 6b, we were able to identify meridian arcs, which are the result of the same (120) and (032) diffraction planes.

Therefore, we can interpret the XRD data from Figure 6b,c as an indication that the PEO is crystalline (agrees with DSC), and the PEO chain in the crystal is perpendicular to the plane of the film surface. This chain orientation of PEO is not observed in films without clay. When 2D XRD data of a PEO−PVP film were collected in both edge and surface orientations, both XRD patterns were found to be identical and showed diffraction rings indicating random orientation throughout the PEO−PVP film. The orientation of the PEO crystal in the clay nanocomposite has to originate from the presence of the intercalated clay. When the nanocomposite films were heated, the melting of PEO crystals was observed with in situ high-temperature XRD measurements, while there was essentially no change in the clay crystal (Figure 7). When the composite film was cooled down after annealing at 150 °C, PEO was seen to recrystallize and resume the orientation as before.

With the use of the diffraction data in Figure 6b,c, several PEO diffraction peaks were measured for their respective d-spacings, allowing for determination of the unit cell parameters for PEO in the nanocomposite film. These unit cell data agree well with the PEO monoclinic unit cell reported in the literature by Takahasi.[59] To gain further knowledge of the composite microstructure, the crystallite size of PEO crystals in the nanocomposite was determined using the Scherrer technique.[60] Table 6 indicates that different crystal planes have different crystal sizes. From the data in Table 6, the crystal size of PEO in the nanocomposite film is ∼200 Å(length) × 200 Å(width) × 100 Å(depth) where the crystal size along the *c*-axis is ∼100 Å. The dimensions are identical to the PEO crystal without the presence of clay. This is consistent with our speculation that PEO crystallizes outside the intercalated clay. Generally speaking, the composite is made of two constituents: the intercalated clay crystal and the PEO crystal. The two constituents in the nanocomposite have a similar *c*-axis-dimension based on Tables

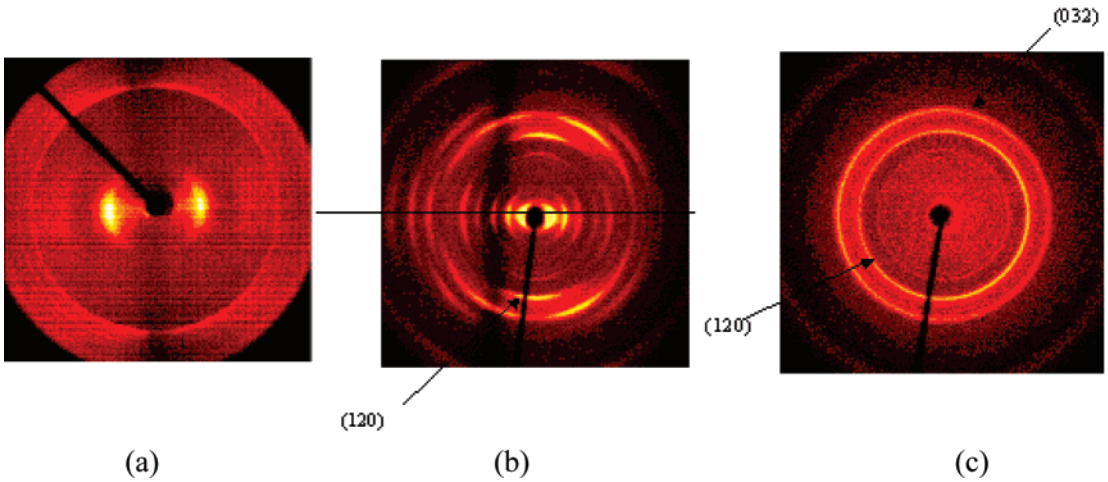

Figure 6. Two-dimensional X-ray diffraction patterns for (a) Cloisite Na^+ clay, edge alignment, (b) PEO−clay(PVP) nanocomposite, 76/12(11) vol ratio, edge alignment, (c) PEO−clay(PVP) nanocomposite, 76/12(11) vol ratio, surface alignment.

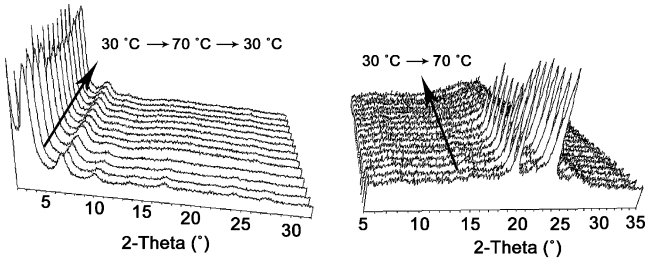

Figure 7. In situ XRD measurement when PEO−clay(PVP) of 76/12(11) volume ratio, composite film was heated: (a) reflection mode with a temperature profile of 30 °C → 70 °C → 0 °C, (b) transmission mode with a temperature profile of 30 °C → 70 °C.

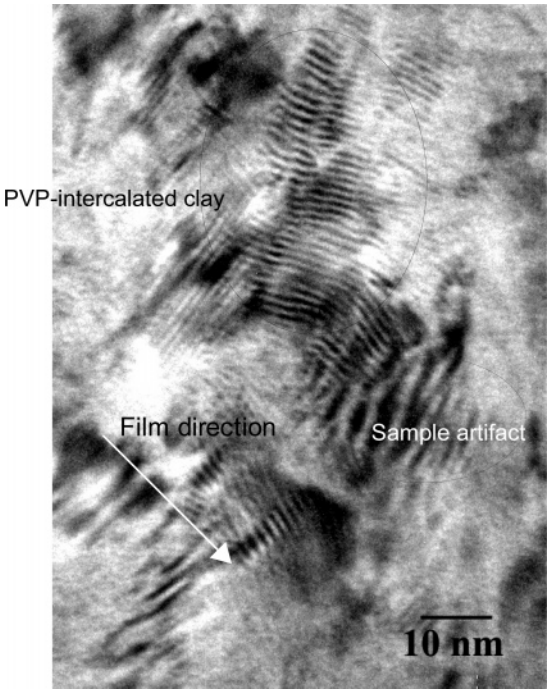

Figure 8. TEM of the cross section of a PEO−clay(PVP) nanocomposite film.

Table 6. Crystallite Size of Peo, the Composition of Peo−Clay(PVP) Is 76/12(11) Volume Ratio

	(hkl) lattice plane	crystallite size (Å)
neat PEO	(120)	223
neat PEO	(032)	146
PEO in PEO−clay(PVP)	(120)	256
PEO in PEO−clay(PVP)	(032)	123

2 and 6. This is speculated to facilitate the mutual templating of the ordering of the two types of crystals in the nanocomposite. In addition, the absorption of the PEO on the edge of the clay sheets also helps to dictate the crystallization growth direction. The PEO crystals and intercalated clay crystals are mixed together with a fixed orientation of the PVP−intercalated clay crystal being parallel to the film plane and the PEO chain axis (*c*-axis) being perpendicular to the film plane.

A TEM micrograph of the cross section of the nanocomposite film shows the ordered layer structure (Figure 8). It shows that the interlayer spacing is ∼25 Å, which is consistent with that for PVP−clay measured by XRD. It also shows the intercalated clays have orientation that is parallel to the film plane.

Figure 3 shows that there is a critical clay volume for synergistic property improvement, which is ∼10 vol % or 20 wt % of clay. One hypothesis to explain this property enhancement is the percolation theory. Percolation phenomenon has been discussed in many two-phase systems and is considered an important factor to contribute to different properties.[61] The critical percolation point, or the phase transition point, is affected by various lattice models.[62] For instance, although the triangular lattice has a percolation concentration of 0.5, the percolation concentration for a bcc (body-centered cubic) or fcc (face-centered cubic) lattice is at a value of 0.2. At 10 vol % clay, the volume ratio of the PEO crystal and PVP−intercalated clay crystal at a PEO−clay(PVP) ratio of 76/12(11) vol % was calculated to be 2.7:1; thus, the volume fraction of the nanofiller is about 0.27. It is likely that the composite reaches percolation at this composition. The properties of the two-phase material often have singular behavior near its critical concentration. Thus the significant property enhancement in the above-discussed composites may originate from the extended filler volume through intercalation and the low-percolation threshold from the composite morphology. This would be a new route to generate nanocomposites with unique properties.

Conclusion

In this paper, it has been shown that a PEO−clay(PVP) nanocomposite film exhibits a low-thermal expansion coefficient of ∼10 ppm/°C, which is similar to that of metals, and an unexpected high-heat distortion temperature that is much higher than the melting point of the PEO. The film also exhibits a much improved O_2 barrier property, high stiffness, and high strength. The significant property improvement is related to the structure of the formed composite. In this composite, the clay crystal is first intercalated by PVP, which regulates the stacking of the clay sheets and helps to form a well-ordered intercalated clay crystal. This intercalated clay crystal as the nanofiller directs the crystallization and crystal orientation of the PEO in the composite.

Acknowledgment. The authors thank Dr. John Minter, Craig Barnes, Janet Fritsch, Nancy Furbeck, Robert Kress, and Dominic Motyl for their assistance with experiments and instruments performed during this study and Dr. Debasis Majumdar for helpful discussions. Y. Rao thanks Drs. Edward Schofield, Robert Daly, and John Pochan for their support of this work.

References and Notes

(1) *Polymer Handbook*; Brandrup, J., Immergut, E. H., Grulke, E.A., Eds.; Wiley: New York, 1999.
(2) *Handbook of Chemistry and Physics*; Weast, R. C., Ed.; CRC Press: Boca Raton, FL, 1977.
(3) Green, D. *An Introduction to the Mechanical Properties of Ceramics*; Cambridge University Press: Cambridge, U.K., 2004.
(4) Boyer, R. F.; Spencer, R. S. *J. Appl. Phys.* **1945**, *16*, 594.
(5) Davis, G. T.; Eby, R. K.; Colson, J. P. *J. Appl. Phys.* **1970**, *41* (11), 4316.
(6) Kardos, J. L.; Raisoni, J.; Piccarolo, S.; Halpin, J. C. *Polym. Eng. Sci.* **1979**, *19* (14), 1000.
(7) Porter, J. *Therm. Anal.* **1975**, *8*, 547.
(8) Mason, P. *Polymer* **1964**, *5* (12), 625.
(9) Fahmy, A. A.; Ragai, A. N. *J. Appl. Phys.* **1970**, *41* (13), 5108.
(10) Fahmy, A. A.; Ragai, A. N. *J. Appl. Phys.* **1970**, *41* (13), 5112.
(11) Turner, P. S. *J. Res. Natl. Bur. Stand. (U.S.)* **1946**, *37*, 239.
(12) Halpin J. C. *J. Compos. Mater.* **1969**, *3*, 732.
(13) Chow T. S. *J. Polym. Sci., Polym. Phys. Ed.* **1978**, *16*, 959 and 967.
(14) Lee, K. Y.; Kim, K. H.; Jeoung, S. K.; Ju, S. I.; Shim, J. H.; Kim, N. H.; Lee, S. G.; Lee, S. M.; Lee, J. K.; Paul, D. R. *Polymer* **2007**, *48*, 4174.
(15) Negi, Y. S.; Goyal, R. K. *Int. J. Plast. Technol.* **2003**, *7* (2), 99.
(16) Yano, K.; Usuki, A.; Okada, A.; Kurauchi, T.; Kamigaito, O. *J. Polym. Sci., Part A: Polym. Chem.* **1993**, *31* (10), 2493.
(17) Lu, Y.; Zhang, G.; Feng, M.; Zhang, Y.; Yang, M.; Shen, D. *J. Polym. Sci., Part B: Polym. Phys.* **2003**, *41* (19), 2313.

(18) Lee, S. H.; Kim, J. E.; Song, H. H.; Kim S. W. *Int. J. Thermophys.* **2004**, *25* (5), 1585.
(19) Karaman, V. M.; Privalko, E. G.; Privalko, V. P.; Kubies, D.; Puffr, R.; Jerome, R. *Polymer* **2005**, *46* (6), 1943.
(20) Koerner, H.; Misra, D.; Tan, A.; Drummy, L.; Mirau, P.; Vaia, R. *Polymer* **2006**, *47*(10), 3426.
(21) Gianelli, W.; Ferrara, G.; Camino, G.; Pellegatti, G.; Rosenthal, J.; Trombini, R. C. *Polymer* **2005**, *46* (18), 7037.
(22) Uhl, F. M.; Davuluri, S. P.; Wong, S.-C.; Webster, D. C. *Chem. Mater.* **2004**, *16* (6), 1135.
(23) Yoon, P. J.; Fornes, T. D.; Paul, D. R. *Polymer* **2002**, *43* (25), 6727.
(24) Privalko, V. P.; Karaman, V. M.; Privalko, E. G.; Lehmann, B.; Friedrich, K. *J. Macromol. Sci., Phys.* **2003**, *B42* (5), 975.
(25) Wong, M.; Paramsothy, M.; Xu, X. J.; Ren, Y.; Li, S.; Liao, K. *Polymer* **2003**, *44* (25), 7757.
(26) Wang, S.; Liang, Z.; Gonnet, P.; Liao, P.; Wang, B.; Zhang, C. *Adv. Funct. Mater.* **2007**, *17* (1), 87.
(27) Guo, H.; Sreekumar, T. V.; Liu, T.; Minus, M.; Kumar, S. *Polymer* **2005**, *46* (9), 3001.
(28) Ge, J. J.; Hou, H.; Li, Q.; Graham, M. J.; Greiner, A.; Reneker, D. H.; Harris, F. W.; Cheng, S. Z. D. *J. Am. Chem. Soc.* **2004**, *126* (48), 15754.
(29) Drzal L. T.; Fukushima H. Nanographite: A Multifunctional Nanomaterial for Polymers and Composites. Presented at High Performance Fillers 2006, The Second International Conference on Fillers for Polymers, Cologne, Germany, March 21−22, 2006; Paper 15/8.
(30) Wu, J.; Yang, S.; Gao, S.; Hu, A.; Liu, J.; Fan, L. *Eur. Polym. J.* **2005**, *41* (1), 73.
(31) Gonsalves K. E.; Chen X.; Baraton M.-I. *Nanostruct. Mater.* **1997**, *9* (1−8), 181.
(32) Schmidt, H. *Macromol. Symp.* **2000**, *59*, 43.
(33) Avella, M.; Bondioli, F.; Cannello, V.; Cosco, S.; Errico, M. E.; Ferrari, A. M.; Focher, B.; Malinconico, M. *Macromol. Symp.* **2004**, *218*, 201.
(34) Sullivan, L. M.; Lukehart, C. M. *Chem. Mater.* **2005**, *8*, 2136.
(35) Chen, W.-Y.; Ho, K. S.; Hsieh, T.-H.; Chang, F.-C.; Wang, Y.-Z. *Macromol. Rapid Commun.* **2006**, *27* (6), 452.
(36) Pramanik, N.; Mohapatra, S.; Pramanik, P.; Bhargava, P. *J. Am. Ceram. Soc.* **2007**, *90* (2), 369.
(37) van Olphen H. *An Introduction to Clay Colloid Chemistry*; Wiley: New York, 1977.
(38) Okada, A.; Usuki, A. *Mater. Sci. Eng.* **1995**, *C3*, 109.
(39) Usuki, A.; Kojima, Y.; Kawasumi, M.; Okada, A.; Fukushima, Y.; Kurauchi, T.; Kamigaito, O. *J. Mater. Res.* **1993**, *8*, 1179.
(40) Usuki, A.; Kojima, Y.; Kawasumi, M.; Okada, A.; Fukushima, Y.; Kurauchi, T.; Kamigaito, O. *J. Mater. Res.* **1993**, *8*, 1185.
(41) Gilman, J. W.; Jackson, C. L.; Morgan, A. B.; Harris, R. H.; Manias, E.; Giannelis, E. P.; Wuthenow, M.; Hilton, D.; Phillips, S. *Chem. Mater.* **2000**, *12*, 1866.
(42) Messersmith, P. B.; Giannelis, E. P. *J. Polym. Sci., Part A: Polym. Chem.* **1995**, *33*, 1047.
(43) Wu, J.; Lerner, M. *Chem. Mater.* **1993**, *5*, 835.
(44) Koo, C. M.; Ham, H. T.; Choi, M. H.; Kim, S. O.; Chung, I. J. *Polymer* **2003**, *44*, 681.
(45) Carrado, K. A.; Xu, L. *Chem. Mater.* **1998**, *10*, 1440.
(46) Majumdar, D.; Blanton, T. N.; Schwark, D. W. *Appl. Clay Sci.* **2005**, *27*, 265.
(47) Vaia, R. A.; Sauer, B. B.; Tse, O. K.; Giannelis, E. P. *J. Polym. Sci., Part B: Polym. Phys.* **1997**, *35*, 59.
(48) Sandi, G.; Joachin, H.; Kizilel, R.; Seifert, S.; Carrado, K. A. *Chem. Mater.* **2003**, *15*, 838.
(49) Dundigalla, A.; Lin-Gibson, S.; Ferreiro, V.; Malwitz, M. M.; Schmidt, G. *Macromol. Rapid Commun.* **2005**, *26*, 143.
(50) Sun, L.; Ertel, E. A.; Zhu, L.; Hsiao, B. S.; Avila-Orta, C. A.; Sics, I. *Langmuir* **2005**, *21* (13), 5672.
(51) Homminga, D.; Coderis, B.; Dolbnya, I.; Reynaers, H.; Groeninckx, G. *Polymer* **2005**, *46*, 11359.
(52) Ogata, N.; Kawakage, S.; Ogihara, T. *J. Appl. Polym. Sci.* **1997**, *66*, 573.
(53) Blanton, T. N.; Majumdar, D.; Melpolder, S. *Mater. Res. Soc. Symp. Proc*. **2000**, *628*, CC11.14.1.
(54) Hosemann, R.; Wilke, W. *Macromol. Chem.* **1968**, *118*, 230.
(55) Hoffman, U.; Edgell, K.; Wilm, D. *Z. Kristallogr.* **1933**, *86*, 340.
(56) Karaborni, S.; Smit, B.; Heidug, W.; Urai, J.; van Oort, E. *Science* **1996**, *271*, 1102.
(57) Gaudiana, R. A.; Sinta, R. F. *J. Polym. Sci., Part A: Polym. Chem.* **1990**, *29*, 45.
(58) Rao, Y. *SPE ANTEC Proceedings*; Society of Plastic Engineers: Brookfield, CT, 2006; Volume 64, p 367.
(59) Takahashi, Y.; Tadokoro, H. *Macromolecules* **1973**, *6*, 672.
(60) Cullity B. D. *Elements of X-ray Diffraction*, 2nd ed.; Addison-Wesley: Reading, MA, 1978.
(61) Katti, K. S.; Sikdar, D.; Katti, D. R.; Shosh, P.; Verma, D. *Polymer* **2006**, *47*, 403.
(62) Stauffer D.; Aharony A. *Introduction to Percolation Theory*; Taylor & Francis: London, U.K., 2001.

MA7020216